

# Performance Evaluation of Palm Kernel Shell as Pitting Corrosion Inhibitor

Nnaemeka Uwaezuoke, Oko Emmanuel Onya, Nnaji Okechukwu Christopher, Chukwuebuka Francis Dike\*, Ibuchukwu Stanley Onwukwe, Federal University of Technology Owerri, Imo State, Nigeria

## Abstract

Pitting corrosion is a critical issue in the petroleum industry, leading to substantial economic losses and environmental hazards, such as equipment failures, product contamination, and catastrophic system breakdowns. The conventional reliance on synthetic corrosion inhibitors, while effective, raises concerns regarding their environmental impact and potential health risks. Moreover, the use of imported inhibitors introduces additional cost and logistical challenges. Recent trends have focused on developing sustainable and environmentally benign alternatives derived from locally available materials. This study evaluates the feasibility of palm kernel shell ash (PKSA), an abundant agricultural byproduct, as an eco-friendly corrosion inhibitor for petroleum production equipment. Experimental results demonstrate that PKSA significantly mitigates corrosion rates, offering a cost-effective and environmentally sustainable alternative to traditional inhibitors. X-ray fluorescence (XRF) analysis reveals that PKSA comprises approximately 27 mol% MgO, 14 mol% SiO<sub>2</sub>, 29 mol% CaO, 7.72mol% K<sub>2</sub>O, and 4.9mol% Al<sub>2</sub>O<sub>3</sub>, compounds known for their corrosion-inhibiting properties. The inhibition mechanism is attributed to the formation of a protective film on the metal surface, composed of calcium and magnesium compounds, which prevents the penetration of aggressive corrosive agents. Corrosion rate reduction is observed through weight loss measurements, with a gradual decline beginning at around 200°C, highlighting the potential of PKSA as a viable corrosion control solution for petroleum systems.

## Introduction

Corrosion presents a significant global challenge in various engineering systems and structural components. Within the petroleum industry, the presence of corrosive substances in crude oil raises concerns about the damage inflicted on pipelines and machinery during production and transportation (Oyewole et al. 2021). Pitting corrosion is characterized by the formation of small, deep pits on metal surfaces, which can compromise the structural integrity of equipment. Mild steel, commonly used in the petroleum industry, is particularly vulnerable to this form of corrosion when exposed to chloride ions in saline environments. The consequences of corrosion are often numerous, and the effects on the safe, reliable and efficient operation of equipment or structures are often more serious than the simple loss of a mass of the metal. Consequently, the need to control corrosion of petroleum production equipment continues to be a major concern to the engineer (Alawode and Ogunleye 2011), as failure of various kinds may occur, and expensive replacements required even though the amount of metal destroyed may be small. Assessing the extent of internal corrosion at the bottom of equipment such as storage tanks can be challenging (Jiang et al. 2017).

Failing to accurately monitor internal corrosion can have catastrophic consequences. As a result, there has been a need for effective corrosion inhibitors in acidizing industries that can be combined with mineral acids

---

Copyright © the author(s). This work is licensed under a Creative Commons Attribution 4.0 International License.

Improved Oil and Gas Recovery

DOI: 10.14800/IOGR.1336

Received December 10, 2024; revised December 22, 2024; accepted December 29, 2024.

\*Corresponding author: [dike.chukwuebuka@futo.edu.ng](mailto:dike.chukwuebuka@futo.edu.ng)

during regular treatment of industrial equipment. A corrosion inhibitor is a substance that slows down the process of corrosion. It is typically added in small amounts to pickling acids in flow systems, such as pipes, either continuously or intermittently. The purpose of using inhibitors is to prevent or reduce the rate of corrosion on metallic materials. These inhibitors work by impeding the partial reactions that cause corrosion through the formation of a dense film layer. This layer acts as a barrier between the corroding surface and the surrounding environment (Oguzie et al. 2013).

One approach that has attracted significant interest is the use of natural compounds as corrosion inhibitors. Unlike traditional synthetic inhibitors, natural extracts offer the advantage of being environmentally friendly and sustainable. Amongst all-natural sources, plants have emerged as particularly promising candidates due to their diverse range of bioactive constituents (Safian et al. 2023). The use of biomaterials in general and agro-waste in particular is a subject of great interest nowadays not only from the technological and scientific points of view, but also socially, and economically, in terms of employment, cost and environmental issues. Bio-wastes are produced from a large variety of sources and agro-wastes are a class of these wastes. Agro-wastes are gotten from animal and plant sources. These wastes contribute to the problem of environmental pollution and the growing cost of handling the problems of environmental pollution is a world problem being tackled by various organizations around the world. Nwaobakata and Agunwamba (2014) suggested that a wise alternative is to utilize these wastes and extract useful substances from them and therefore reduce the cost of disposing the wastes and the environmental damages imposed on our environment by these wastes. This has led to their synthesis to nanoparticles form Uwaezuoke (2022) and utilization as alternatives for conventional materials in drilling (Uwaezuoke et al. 2022), production and enhanced oil recovery. Most of these inhibitors are organic compounds that contain nitrogen, sulfur or oxygen atoms within their structures. They work by absorbing onto the metal surface and creating a protective barrier against corrosive attacks (Umoren et al. 2016).

Several plants have been utilized by corrosion inhibitors by several authors. Kumar and Mohana (2014) utilized pterolobium hexpetalum and celosia argentea for corrosion inhibition using weight loss and electrochemical impedance spectroscopy. From the result of their study there was an increase in inhibition efficiency with increase in concentration and decrease in inhibition efficiency with increase in temperature. Chevalier et al. (2014) conducted a corrosion inhibition study in HCL using anibaros aeodora at constant temperature. From the result of their experimental study the increase in concentration yielded an increase in inhibition efficiency. Chigondo and Chigondo (2016) carried out a corrosion inhibition study in salt water environment using neem as material and weight loss as evaluation method. From the result of their experimental study, Hussain et al. (2016) carried a corrosion inhibition study in HCL environment using elaeis guineensis as material, and weight loss, potentiodynamic polarization & electrochemical impedance spectroscopy as method. The result of their experimental increase in temperature yielded reduction in inhibition efficiency while increase concentration yielded increase in inhibition efficiency. Murthy and Vijayaragavan (2017) carried out corrosion inhibition by weight loss test in H<sub>2</sub>SO<sub>4</sub> and HCl environment using hibiscus sabdariffa. From the result of their experimental study, increase in concentration yielded increase inhibition efficiency. Chinwego (2017) carried out corrosion inhibition study in NaCl using a blend of palm and jatropha leaf. From the result of the experimental study, the palm-jatropha lead blend yielded inhibition efficiency of 60.9%.

This study focuses on the use of locally sourced materials available in regions with significant petroleum production activities. The evaluation of carbon steel corrosion in the produced water of crude oil is of great interest to the petrochemical industry due to costly economic and human losses (Deyab and Abd El-Rehim 2014). Carbon steel is the most economical and common material used in the oil and gas industry (Deyab et al. 2016). Large amounts of palm kernel shells are produced during the extraction of palm oil from palm fruits and these shells must be used for a variety of purposes. Research is currently being conducted on a variety of topics, such as the use of palm kernel shells as an additive in drilling fluids, livestock feed, construction aggregates, reinforcement for metals and polymeric composites, wastewater detoxifier, abrasive in automotive components, and bioenergy (Borah and Das 2022; Saad et al. 2021).

By utilizing these materials, the research promotes sustainable practices and reduces the reliance on imported chemical inhibitors. The study is conducted using mild steel samples, a standard material in the petroleum industry, and simulates saline environments to replicate actual operational conditions. The findings of this study are expected to contribute to the development of cost-effective and environmentally friendly corrosion inhibitors. This research has the potential to influence corrosion management strategies in the petroleum industry and reduce the environmental impact of corrosion.

## Methodology

The methodology for this study involves the preparation and testing of mild steel samples in a controlled laboratory environment. The experimental setup includes the following parts.

**Collection of Samples.** Palm kernel shells (**Figure 1**) were obtained from Eziobodo in Owerri, Imo State Nigeria.



**Figure 1—Palm kernel shell.**

**Preparation of Mild Steel and Palm Kernel Shell Ash.** The palm kernel shell was cleaned and dried, they were packed in graphite crucible and crushed to obtained palm kernel shell ash **Figure 2**.



**Figure 2—Palm kernel shell particulate.**

**Production of Nanoparticles.** The sol gel method was applied in producing the palm kernel shell ash nanoparticles. 50g of Sodium hydroxide mixed in one dm<sup>3</sup> of water was added to 100 g of Palm kernel ash, put in an Erlenmeyer flask and stirred for about 2 hours before the solution was filtered to remove the residue which is carbon **Figure 3**. The filtrate was then allowed to cool at room temperature, then hydrochloric acid of weight 0.5 mols was added and stirred for hydrolysis - condensation reaction to occur until pH of 7 was attained with a pH meter and ageing was done at 65°C for 8 hours in an oven to obtain the gel.



Figure 3—The palm kernel shell ash filtrate.

**Characterization of Nanoparticles.** The size of the nanoparticles as well as their form and structure were observed with Scanning Electron Microscope, X-ray fluorescence spectrometer was utilized for the composition analysis of the produced nanoparticles, X-ray diffractometer, XPertPro PANalytical, LR 39487C was used to obtain the X-ray diffraction patterns of Palm kernel ash nanoparticles. Sample weight of 10 mg was heated from 10 to 861°C with a heating rate of 10°C/min in nitrogen atmosphere. Thermal gravimetric analysis (TG) was assessed using Perkin-Elmer Pyris 6 TGA analyzer. Morphology and particle dimension of produced nano-silica were observed with an SEM (Zeiss Ultra Plus) and EDX at Secondary Electron Image (SEI) and high vacuum (HV) mode with 20 kV accelerating voltage. The analysis was performed using an Rh (rhodium) anode or source, with an X-ray energy of 30.0 keV and a silicon drift detector (SDD) type filter. The concentrations were calibrated or quantified using a specific method which was the Gaussian fitting approach.

## Results

The experimental results demonstrate that all three inhibitors significantly reduce the corrosion rate of mild steel in a saline environment. Coconut shell ash and neem leaves extract exhibit mixed-type inhibition behavior, affecting both anodic and cathodic reactions. Periwinkle shell powder primarily influences the cathodic reaction by reducing hydrogen evolution.

**X-RAY Fluorescence (XRF) Analysis.** As an analytical technique, XRF identifies the presence and proportion of elements in a material so that the chemical composition can be established. Remarkably, **Table 1** shows calcium oxide, magnesia silica, alumina and potassium oxide as the major components of the sample. The high silica, magnesia and alumina contents imply potential inhibition property which reveals why ash generated from PKS has been studied as a potential corrosion inhibitor for petroleum equipment.

**Table 2** presents oxygen, calcium, magnesium and silicon as the major elemental constituents of PKS as well as aluminum and phosphorus. Calcium oxide (CaO) also known as quicklime and which form 29.34 mol% of the sample, can react with water to form calcium hydroxide which can help neutralize acidic corrosive substances like hydrogen sulfide and carbon dioxide to form neutral substances, reducing their corrosive effects and protecting the metal surfaces from corrosion.

Silica (SiO<sub>2</sub>) which forms 14 mol% of the sample and is also known as silicon dioxide can help inhibit corrosion by forming a protective layer on metal surfaces, reducing the reactivity of the metal and preventing the formation of corrosive compounds. Silica has a high affinity for water and can help reduce moisture levels, making it more difficult for corrosive substances to form.

**Table 1—Percentage chemical composition (by weight) of PKS from XRF analyses.**

| Layer | Component                      | Type | Concn  | Error  | Units | Mole%  | Error  |
|-------|--------------------------------|------|--------|--------|-------|--------|--------|
| 1     | SiO <sub>2</sub>               | Calc | 13.091 | 2.162  | wt.%  | 14.014 | 2.315  |
| 1     | V <sub>2</sub> O <sub>5</sub>  | Calc | 0.016  | 0.077  | wt.%  | 0.006  | 0.027  |
| 1     | Cr <sub>2</sub> O <sub>3</sub> | Calc | 0.025  | 0.052  | wt.%  | 0.010  | 0.022  |
| 1     | MnO                            | Calc | 0.206  | 0.050  | wt.%  | 0.186  | 0.045  |
| 1     | Fe <sub>2</sub> O <sub>3</sub> | Calc | 8.380  | 0.170  | wt.%  | 3.375  | 0.069  |
| 1     | Co <sub>3</sub> O <sub>4</sub> | Calc | 0.068  | 0.060  | wt.%  | 0.018  | 0.016  |
| 1     | NiO                            | Calc | 0.013  | 0.041  | wt.%  | 0.011  | 0.035  |
| 1     | CuO                            | Calc | 0.323  | 0.042  | wt.%  | 0.261  | 0.034  |
| 1     | Nb <sub>2</sub> O <sub>3</sub> | Calc | 0.071  | 0.046  | wt.%  | 0.020  | 0.013  |
| 1     | MoO <sub>3</sub>               | Calc | 0.034  | 0.054  | wt.%  | 0.015  | 0.024  |
| 1     | WO <sub>3</sub>                | Calc | 0.044  | 0.167  | wt.%  | 0.012  | 0.046  |
| 1     | P <sub>2</sub> O <sub>5</sub>  | Calc | 7.987  | 0.969  | wt.%  | 3.619  | 0.439  |
| 1     | SO <sub>3</sub>                | Calc | 3.680  | 0.546  | wt.%  | 2.956  | 0.438  |
| 1     | CaO                            | Calc | 25.587 | 0.654  | wt.%  | 29.348 | 0.750  |
| 1     | MgO                            | Calc | 17.211 | 29.342 | wt.%  | 27.466 | 46.825 |
| 1     | K <sub>2</sub> O               | Calc | 11.304 | 0.440  | wt.%  | 7.719  | 0.301  |
| 1     | BaO                            | Calc | 0.000  | 0.000  | wt.%  | 0.000  | 0.000  |
| 1     | Al <sub>2</sub> O <sub>3</sub> | Calc | 7.696  | 5.624  | wt.%  | 4.855  | 3.548  |
| 1     | Ta <sub>2</sub> O <sub>5</sub> | Calc | 0.078  | 0.156  | wt.%  | 0.011  | 0.023  |
| 1     | TiO <sub>2</sub>               | Calc | 0.694  | 0.118  | wt.%  | 0.559  | 0.095  |
| 1     | ZnO                            | Calc | 0.267  | 0.039  | wt.%  | 0.211  | 0.031  |
| 1     | Ag <sub>2</sub> O              | Calc | 0.048  | 0.266  | wt.%  | 0.013  | 0.074  |
| 1     | Cl                             | Calc | 2.847  | 0.243  | wt.%  | 5.166  | 0.441  |
| 1     | ZrO <sub>2</sub>               | Calc | 0.062  | 0.046  | wt.%  | 0.032  | 0.024  |
| 1     | SnO <sub>2</sub>               | Calc | 0.268  | 1.920  | wt.%  | 0.114  | 0.819  |

**Table 2—Elements information.**

| Element | Line Code | Cond Code | Ratio Method | Intensity (c/s) | Error (c/s) | Intensity Method | Conc   | Conc Method | Calibration Coefficient |
|---------|-----------|-----------|--------------|-----------------|-------------|------------------|--------|-------------|-------------------------|
| O       | Ka        | 0         | None         | 0.000           | 0.0000      | Gaussian         | 36.474 | None        | 0.000                   |
| Mg      | Ka        | 1         | None         | 1.754           | 2.9903      | Gaussian         | 10.380 | FP          | 0.000                   |
| Al      | Ka        | 1         | None         | 6.699           | 4.8948      | Gaussian         | 4.073  | FP          | 0.000                   |
| Si      | Ka        | 1         | None         | 56.493          | 9.3315      | Gaussian         | 6.119  | FP          | 0.000                   |
| P       | Ka        | 1         | None         | 102.801         | 12.4708     | Gaussian         | 3.486  | FP          | 0.000                   |
| S       | Ka        | 1         | None         | 78.302          | 11.6121     | Gaussian         | 1.474  | FP          | 0.000                   |
| Cl      | Ka        | 1         | None         | 191.786         | 16.3779     | Gaussian         | 2.847  | FP          | 0.000                   |
| K       | Ka        | 1         | None         | 847.580         | 33.0175     | Gaussian         | 9.384  | FP          | 0.000                   |
| Ca      | Ka        | 1         | None         | 1850.114        | 47.3105     | Gaussian         | 18.287 | FP          | 0.000                   |
| Ti      | Ka        | 1         | None         | 65.336          | 11.1164     | Gaussian         | 0.416  | FP          | 0.000                   |
| V       | Ka        | 1         | None         | 1.896           | 9.1934      | Gaussian         | 0.009  | FP          | 0.000                   |
| Cr      | Ka        | 1         | None         | 4.700           | 9.9539      | Gaussian         | 0.017  | FP          | 0.000                   |
| Mn      | Ka        | 1         | None         | 54.823          | 13.3120     | Gaussian         | 0.159  | FP          | 0.000                   |
| Fe      | Ka        | 1         | None         | 2408.342        | 48.9013     | Gaussian         | 5.861  | FP          | 0.000                   |
| Co      | Ka        | 1         | None         | 24.437          | 21.3226     | Gaussian         | 0.050  | FP          | 0.000                   |
| Ni      | Ka        | 1         | None         | 4.961           | 15.5713     | Gaussian         | 0.010  | FP          | 0.000                   |
| Cu      | Ka        | 1         | None         | 142.870         | 18.7667     | Gaussian         | 0.258  | FP          | 0.000                   |
| Zn      | Ka        | 1         | None         | 131.957         | 19.4233     | Gaussian         | 0.214  | FP          | 0.000                   |
| Zr      | Ka        | 1         | None         | 23.897          | 17.8785     | Gaussian         | 0.046  | FP          | 0.000                   |
| Nb      | Ka        | 1         | None         | 26.194          | 17.0293     | Gaussian         | 0.057  | FP          | 0.000                   |
| Mo      | Ka        | 1         | None         | 10.310          | 16.0164     | Gaussian         | 0.023  | FP          | 0.000                   |
| Ag      | Ka        | 1         | None         | 1.943           | 10.8470     | Gaussian         | 0.044  | FP          | 0.000                   |
| Sn      | La        | 1         | None         | 5.743           | 41.1054     | Gaussian         | 0.211  | FP          | 0.000                   |
| Ta      | La        | 1         | None         | 9.752           | 19.4500     | Gaussian         | 0.064  | FP          | 0.000                   |

Alumina ( $\text{Al}_2\text{O}_3$ ) also known as aluminum oxide, forms 4.9 mol% of our sample, and can also form a thin, impermeable layer on metal surfaces, preventing corrosive substances from penetrating. Potassium Oxide ( $\text{K}_2\text{O}$ ) which forms 7.7 mol% also has the same effect and can also be used to enhance protective coatings and paints by enhancing their barrier properties. Alumina's hardness and chemical inertness make it an effective barrier against corrosion. Alumina can also inhibit pitting corrosion by reducing the formation of pits and crevices, which can lead to localized corrosion.

Magnesia ( $\text{MgO}$ ), also known as magnesium oxide which forms 27.466 mol% of the sample is known for its protective properties and can form a barrier against corrosive substances. It is often used in coatings and paints to protect metal surfaces from corrosion. Magnesia and Calcium Oxide have antimicrobial properties which can inhibit the growth of microorganisms that contribute to microbial corrosion. The presence of these elements in the sample shows that palm kernel shell ash can serve in coatings and paints, additives in drilling and production fluids, corrosion inhibition in pipeline transportation, protection lines and wraps, high temperature and pressure environments and corrosive environments with acidic substances to reduce equipment damage, extend lifespan and minimize downtime. Furthermore, its availability and affordability together with other properties like relatively high porosity, surface area and strength-to-weight ratio makes the agricultural waste a potential solid biocatalyst (Nwosu-Obieogua et al. 2022).

**Xrd Crystallinity Analysis.** The compositional analysis of PKS provides a background understanding of its chemical configuration. **Figure 4** presents a comparison between XRD crystallinity analysis of raw PKS and activated carbon from PKS. XRD patterns of raw PKS demonstrated the coexistence of carbon and oxygen atoms at peaks of  $2\theta = 22^\circ$ ,  $28^\circ$  and  $52^\circ$  respectively **Figure 4**.

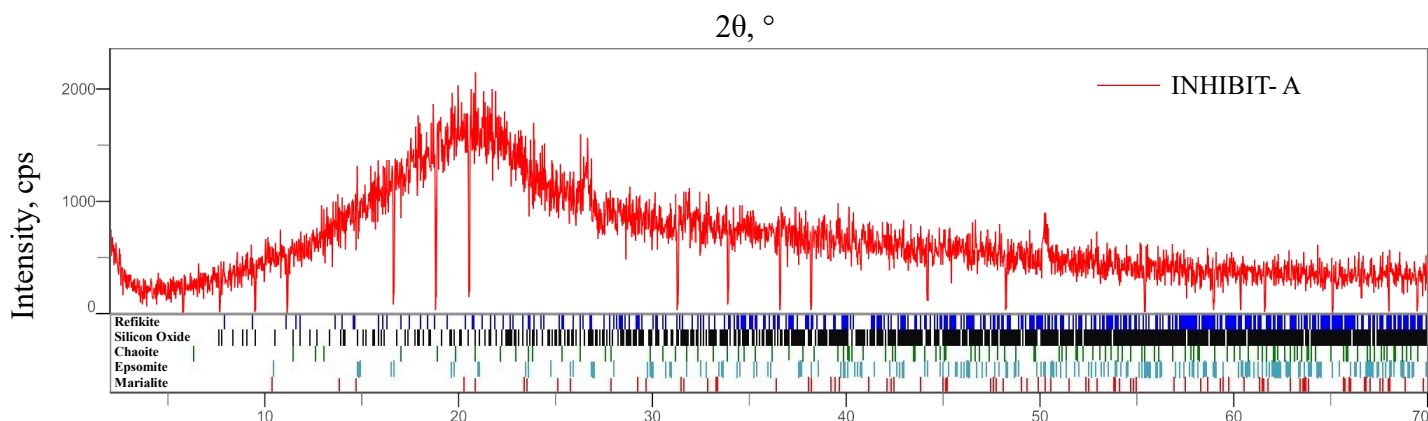


**Figure 4—XRD crystallinity analysis.**

**Figure 5** shows the percentage composition of the minerals in the sample. For instance, results showed that the sample is 53% Refikite, with figure of merit of 5%. Similarly, it is 2.9% Epsomite with figure of merit of 3%.

In **Figure 6**, the peaks represent refikite, epsomite and marialiate between  $2\theta = 15^\circ$  and  $20^\circ$  respectively due to the impurities during the preparation of the sample from the PKS. The broad XRD array of extracted silica nanoparticles at theta =  $15^\circ$ , which is distinctive of amorphous solid, confirms the formation of amorphous silica; similar results were obtained by other researchers (Sapawe et al. 2018). Other peaks at  $2\theta = 11^\circ$ ,  $32^\circ$ ,  $42^\circ$  and  $55^\circ$  represent the nature of the PKS nanoparticles and is consistent with other studies (Imoisili et al. 2020; Ikubanni et al. 2020; Jabarullah et al. 2021).



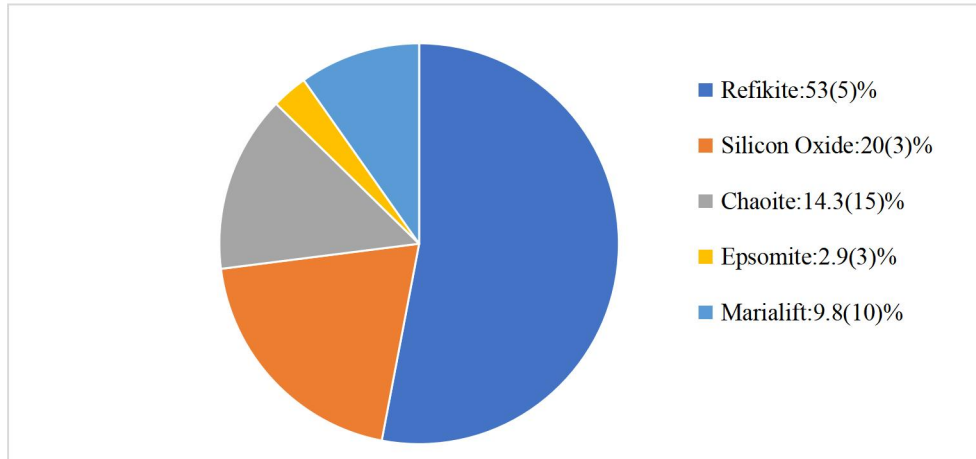


Figure 5—Percentage composition of the minerals in the PKS sample tested.

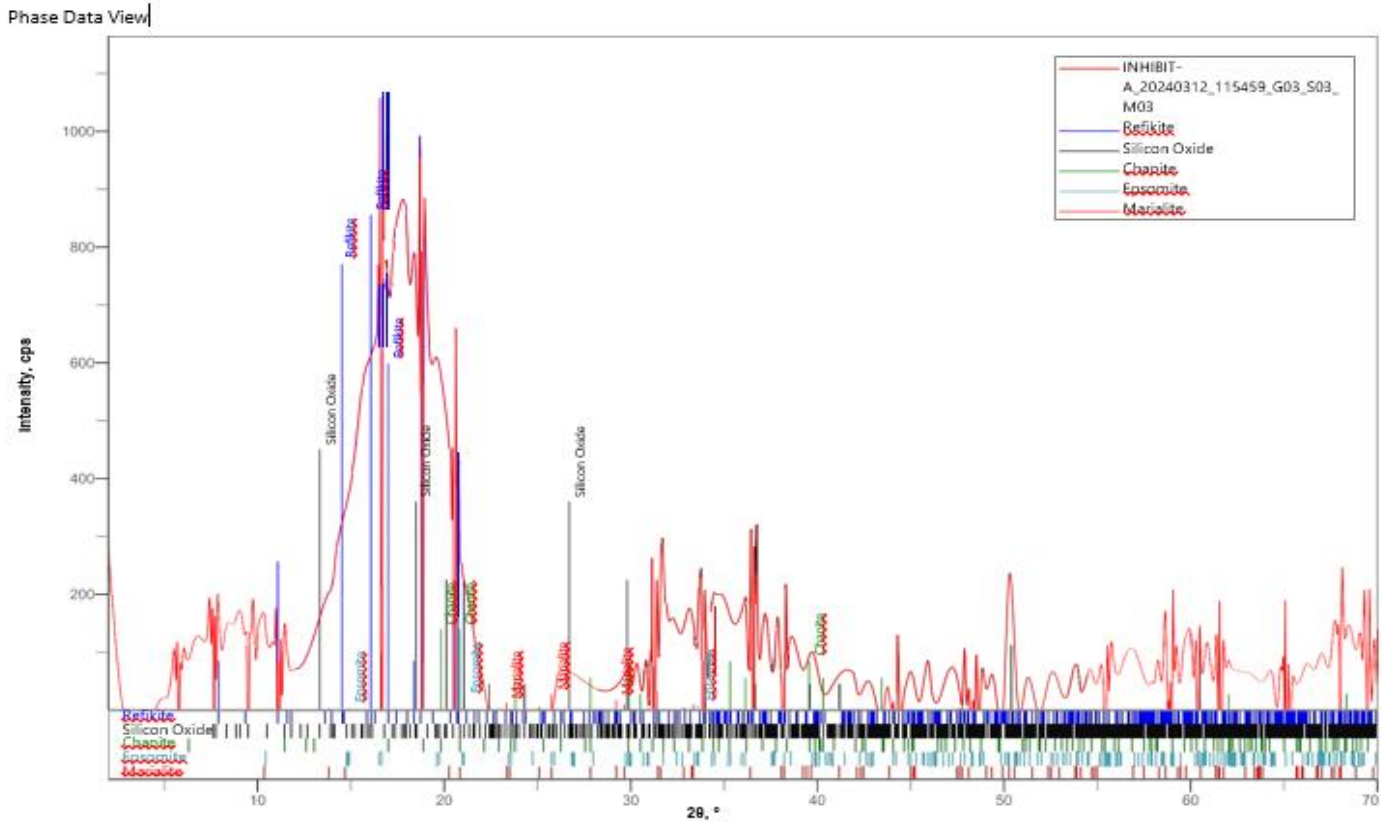


Figure 6—Phase data view.

Table 3 shows the evaluation report of the samples for more a detailed information. For instance, it revealed the presence of Epsomite and Refikite as the peak values of Figure 6, while the qualitative analysis output (Table 4) showed Refikite, Silicon oxide, Chaoite, Epsomite, and Marialite. The values in parenthesis show figures of merit.



**Table 3—Peak list.**

| No.                 | 1                                      | 2   |
|---------------------|--|---|
| 2 $\theta$ , °      | 17.76(9)                               | 18.63(2)  |
| d, Å                | 4.99(3)                                | 4.758(6)  |
| Height, cps         | 424(53)                                | 545(61)   |
| FWHM, °             | 2.9(3)                                 | 0.32(19)  |
| Int. I., cps°       | 1472(157)                              | 259(47)   |
| Int. W., °          | 3.5(8)                                 | 0.47(14)  |
| Asymmetry           | 5(3)                                   | 5(12)   |
| Decay( $\eta$ H/mH) | 0.4(3)                                 | 1(2)  |
| Size, Å             | 29(3)                                  | 266(162)  |
| Phase Name          | Epsomite: 201                          | Refikite: 131, Silicon Oxide                                      |
| Chemical Formula    | MgSO <sub>4</sub> · 7 H <sub>2</sub> O | C <sub>20</sub> H <sub>32</sub> O <sub>2</sub> , SiO <sub>2</sub> |
| Norm. I.            | 100                                    | 17.56   |
| Profile Type        | Split pseudo-Voigt                     | Split pseudo-Voigt  |

**Table 4—Qualitative analysis results.**

| Phase name    | Formula  | Figure of merit |
|---------------|--|-----------------|
| Refikite      | C <sub>20</sub> H <sub>32</sub> O <sub>2</sub>                                 | 0.892           |
| Silicon Oxide | SiO <sub>2</sub>   | 1.238           |
| Chaoite       | C  | 2.850           |
| Epsomite      | MgSO <sub>4</sub> · 7H <sub>2</sub> O  | 2.750           |
| Marialite     | (Na <sub>3.35</sub> Ca <sub>0.38</sub> K <sub>0.24</sub> ) ( Si <sub>8</sub> ) | 2.752           |

TGA measures the weight loss of a material as a function of temperature, which can provide information about thermal stability, decomposition, and phase transformations. The results of thermal gravimetric analysis (TGA) are shown in **Figure 7**. The curve shows a gradual weight loss starting around 200°C, with a more significant weight loss occurring between 400°C and 600°C, suggesting potential decomposition or phase changes of some of these calcium silicate or calcium aluminosilicate compounds present in the sample within this temperature range. Two-step weight losses were observed. The loss in weight up to 310°C (step 1) is ascribed to dehydration caused by the loss of physically adsorbed H<sub>2</sub>O. However, chemically bound water from the sol-gel production method was ascribed to the loss in weight from 330 to 500°C (step 2) (Mueller et al. 2003). Above 550°C, no further weight loss was observed indicating thermal stability of extracted nano silica.

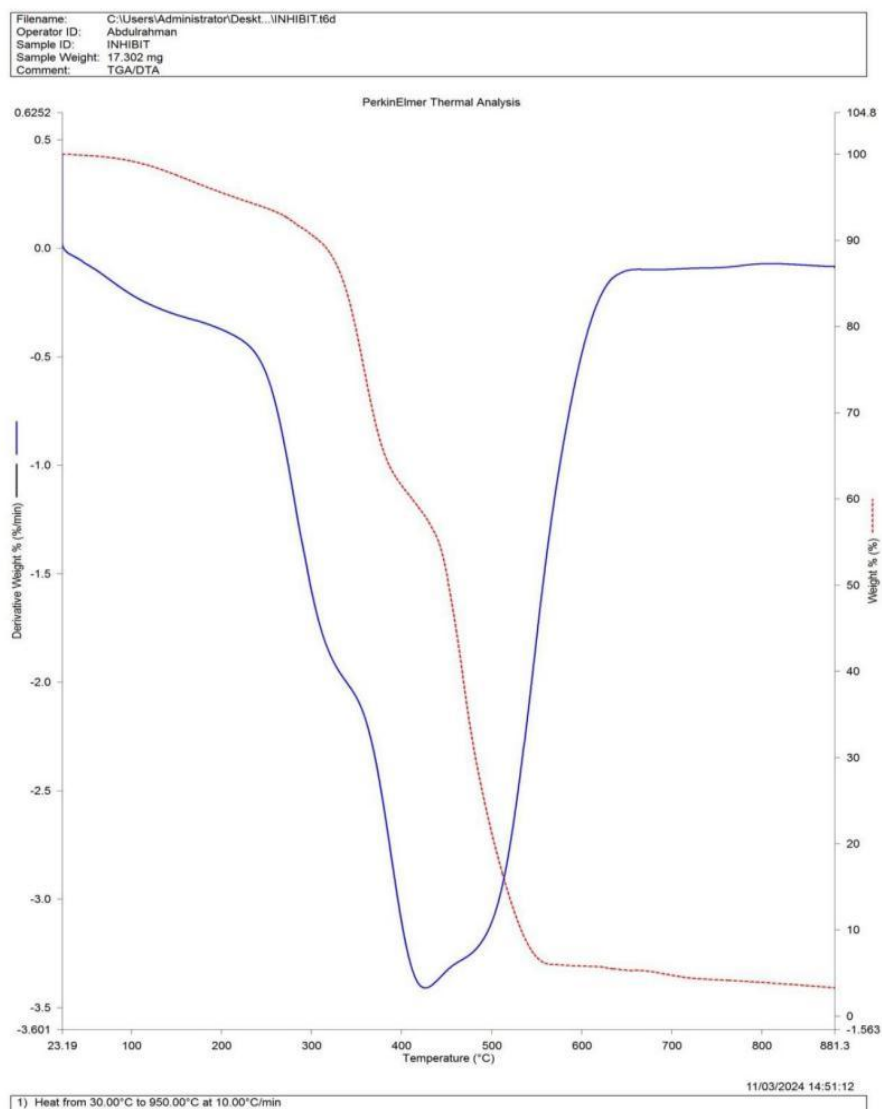


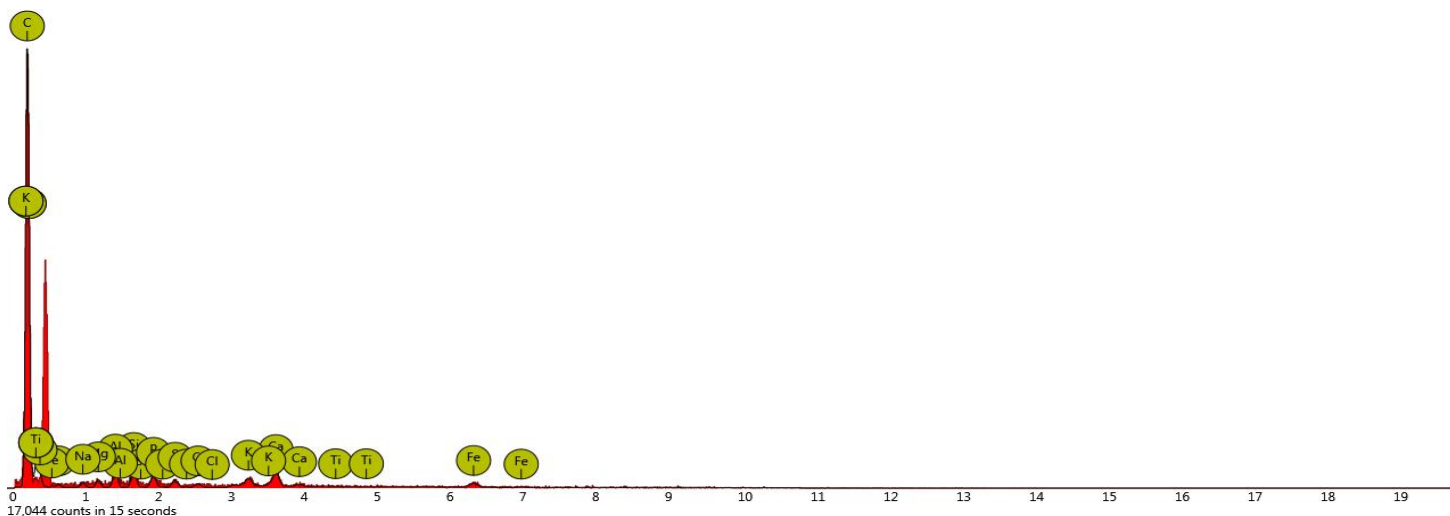
**Figure 7—Thermo-gravimetric analysis of palm kernel shell.**

The thermal behaviour of PKS shows that the agricultural waste decomposes under heat in two stages due to its constituents. The first stage occurs at an onset of 10 °C up until 205 °C with weight loss attributed to vaporization of moisture content. The second stage is initiated at 250 °C and lasts up to 635 °C with one distinct derivative thermo-gravimetric (DTG) peaks which occurs at T=400 °C and marks the onset of the decomposition of hemicellulose and degradation of cellulose (Acevedo-Paez et al. 2019). **Table 5** shows the elemental composition in terms of atomic and weight concentrations. It is possible to say that carbon is the dominant element. With the carbon, it is also possible to infer that nanomaterials such as carbon nanotubes (CNTs) and graphenes etc could be found, which could enhance its performance as corrosion control material.

**Table 5—Atomic concentrations of elements in analyzed sample.**

| Element Number | Element Symbol | Element Name | Atomic Conc. | Weight Conc. |
|----------------|----------------|--------------|--------------|--------------|
| 6              | C              | Carbon       | 81.31        | 74.21        |
| 7              | N              | Nitrogen     | 15.01        | 15.98        |
| 26             | Fe             | Iron         | 0.53         | 2.26         |
| 20             | Ca             | Calcium      | 0.63         | 1.93         |
| 14             | Si             | Silicon      | 0.48         | 1.02         |
| 13             | Al             | Aluminium    | 0.49         | 1.00         |
| 19             | K              | Potassium    | 0.30         | 0.88         |
| 15             | P              | Phosphorus   | 0.37         | 0.86         |
| 16             | S              | Sulfur       | 0.24         | 0.60         |
| 12             | Mg             | Magnesium    | 0.27         | 0.49         |
| 11             | Na             | Sodium       | 0.25         | 0.44         |
| 17             | Cl             | Chlorine     | 0.12         | 0.34         |
| 22             | Ti             | Titanium     | 0.00         | 0.00         |

**Scanning Electron Microscopy (SEM).** Figure 9 shows the EDS of the Microstructure of the PKSA np. As observed from Figure 9, the dominant element is carbon. SEM imaging has been used to study the morphology of the PKSA sample. The morphology of the Palm kernel shell ash nanoparticles (PKSA np) by Scanning electron microscope/energy dispersive spectrometry (SEM/EDS) is shown in Figure 10. It shows the SEM micrograph of silica nanoparticles produced from palm kernel shell ash at  $\times 200,000$  magnification. The particles were observed to be spherical in shape with reduced silica-silica agglomeration. The organic molecules in the waste contain C and O which may provide electron pairs for the waste to adsorb onto the metallic surface. This would lead to a partial blockage of the metal and as a result, limit corrosion in the aggressive solution (Thakur and Kumar 2021). It is feasible to suggest that this waste belongs to the class of inhibitory compounds because it contains both C and O atoms.

**Figure 9—EDS of the Microstructure of the PKSA np.**

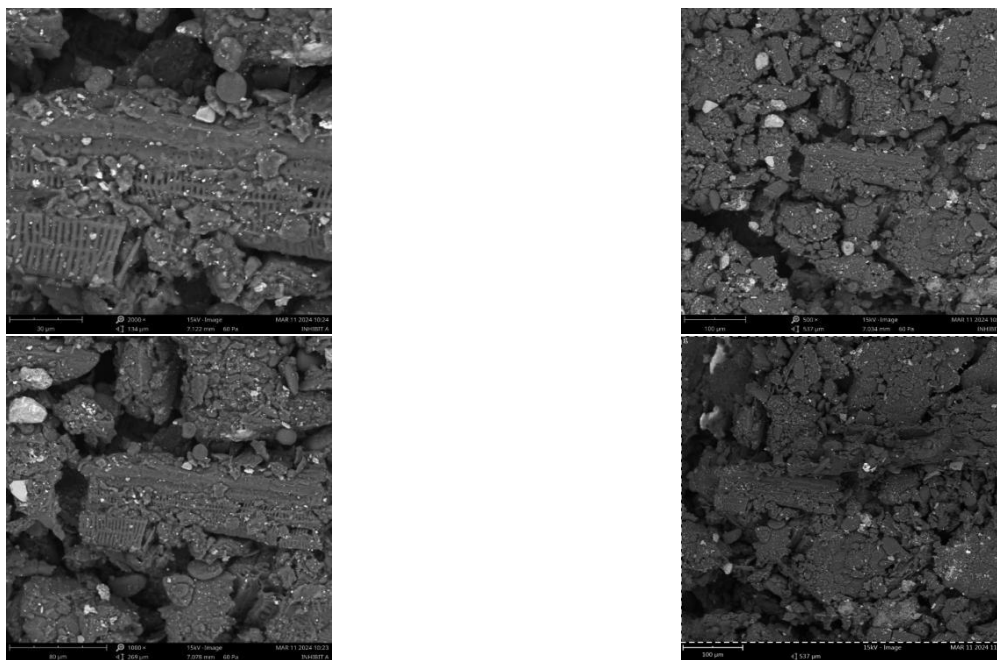


Figure 10—SEM image of samples.

## Conclusions

This research demonstrates the potential of locally sourced materials in inhibiting pitting corrosion on petroleum production equipment. The results demonstrate that PKSA is an effective corrosion inhibitor containing about 27 mol% Magnesia, 14 mol% Silica, 29 mol% CaO, 7.72 mol% K<sub>2</sub>O and 4.9 mol% Alumina, which are all compounds with high capacity for corrosion inhibition. The inhibition mechanism is attributed to the formation of a protective layer on the metal surface, comprising calcium and magnesium compounds present in PKSA.

## Conflicting Interests

The author(s) declare that they have no conflicting interests.

## References

- Alawode, A.J. and Ogunleye, I.O. 2011. Maintenance, Security and Environmental Implications of Pipeline Damage and Ruptures in the Niger Delta Region. *Pacific Journal of Science and Technology* **12(1)**:565-573.
- Acevedo-Paez, J., Duran, J.M., Posso, F., et al. 2019. Hydrogen Production from Palm Kernel Shell: Kinetic Modeling and Simulation. *Int. J. Hydrogen Energy* **44(1)**:123-130.
- Borah, B. and Das, B.M. 2022. A Review on Applications of Bio-Products Employed in Drilling Fluids to Minimize Environmental Footprint. *Environ. Challenges* **6(1)**:100411.
- Chevalier, M., Robert, F., Amusant, N., et al. 2014. Enhanced Corrosion Resistance of Mild Steel in 1 M Hydrochloric Acid Solution by Alkaloids Extract from *Aniba Rosaedora* Plant: Electrochemical, Phytochemical and XPS Studies. *Electrochimica Acta* **131**:96-105.
- Chigondo, M. and Chigondo, F. 2016. Recent Natural Corrosion Inhibitors for Mild Steel: An Overview. *Journal of Chemistry* **2016(1)**:1-9.
- Chinwego, C.A. 2017. Sweet Corrosion Inhibition of Carbon Steel Using a Blend of Palm-Jatropha Leaf Extract in 3.5% NaCl Solution. M.Eng. Thesis, African University of Science and Technology.

- Deyab, M.A. and Abd El-Rehim, S.S. 2014. Effect of Succinic Acid on Carbon Steel Corrosion in Produced Water of Crude Oil. *J. Taiwan Inst. Chem. Eng.* **45(1)**:1065-1072.
- Deyab, M.A., Eddahaoui, K., Essehli, R., et al. 2016. Experimental Evaluation of New Inorganic Phosphites as Corrosion Inhibitors for Carbon Steel in Saline Water from Oil Source Wells. *Desalination* **383**:38-45.
- Hussain, M.H., Rahim, A.A., Ibrahim, M.N.M., et al. 2016. The Capability of Ultrafiltrated Alkaline and Organosolv Oil Palm (*Elaeis Guineensis*) Fronds Lignin as Green Corrosion Inhibitor for Mild Steel in 0.5 M HCl Solution. *Measurement* **78(1)**:90-103.
- Imoisili, P.E., Ukoba, K.O., Jen, T., et al. 2020. Synthesis and Characterization of Amorphous Mesoporous Silica from Palm Kernel Shell Ash. *Bol. Soc. Esp. Ceram. Vidrio* **59(1)**:159-164.
- Ikubanni, P.P., Oki, M., Adeleke, A.A., et al. 2020. Influence of Temperature on the Chemical Compositions and Microstructural Changes of Ash Formed from Palm Kernel Shell. *Results Eng.* **8(1)**:173-201.
- Jabarullah, N.H., Kamal, A.S., Othman, R., et al. 2021. A Modification of Palm Waste Lignocellulosic Materials into Biographite Using Iron and Nickel Catalyst. *Processes* **9(1)**:1079-1091.
- Jiang, T., Ren, L., Jia, Z.G., et al. 2017. Pipeline Internal Corrosion Monitoring Based on Distributed Strain Measurement Technique. *Struct. Control Health Monit.* **24(1)**:2016-2032.
- Kumar, P. and Mohana, K.N. 2014. Phytochemical Screening and Corrosion Inhibitive Behavior of *Pterolobium Hexapetalum* and *Celosia Argentea* Plant Extracts on Mild Steel in Industrial Water Medium. *Egyptian Journal of Petroleum* **23(2)**:201-211.
- Mueller, R., Kammler, H.K., Wegner, K., et al. 2003. OH Surface Density of SiO<sub>2</sub> and TiO<sub>2</sub> by Thermogravimetric Analysis. *Langmuir* **19(1)**:160-165.
- Murthy, Z.V.P. and Vijayaragavan, K. 2017. Mild Steel Corrosion Inhibition by Acid Extract of Leaves of *Hibiscus Sabdariffa* as a Green Corrosion Inhibitor and Sorption Behavior. *Green Chemistry Letters and Reviews* **7(1)**:209-219.
- Nwaobakata, C. and Agunwamba, J.C. 2014. Effect of Palm Kernel Shells Ash as Filler on the Mechanical Properties of Hot Mix Asphalt. *Archives of Applied Science Research* **6(5)**:42-49.
- Nwosu-Obieogua, K., Agu, C.M., Dzarma, G.W., et al. 2022. Microwave-Assisted Carbon-Based Sulphonated Melon Seed Peel Catalyst Development for the Optimization of Neem Seed Oil Epoxidation Using Response Surface Methodology. *Clean Mater* **4(1)**:1-18.
- Oguzie, E.E., Iheabunike, Z.O., Oguzie, K.L., et al. 2013. Corrosion Inhibiting Effect of *Aframomum Meleguta* Extracts and Adsorption Characteristics of the Active Constituents on Mild Steel in Acidic Media. *J. Dispersion Sci. Tech.* **34(1)**:516-527.
- Oyewole, O., Adeoye, J.B., Udoh, V.C., et al. 2023. Optimization and Corrosion Inhibition of Palm Kernel leaves on mild steel in Oil and Gas Applications. *Egyptian Journal of Petroleum* **32(1)**: 41-46.
- Saad, H., Omoleiyomi, B.D., Alhassan, E.A., et al. 2021. Mechanical Performance of Abrasive Sandpaper Made with Palm Kernel Shells and Coconut Shells. *J. Mech. Behav. Mater.* **30(1)**:28-37.
- Safian, M.T., Raja, P.B., Shen, C.Y., et al. 2023. A Novel Preparation of Bio-Based Graphene from Oil Palm Biomass as a Fluid Loss Additive in Water-Based Drilling Fluid. *Geoenergy Sci. Eng.* **231(1)**:212321.
- Sapawe, N., Osman, N.S., Zakaria, M.Z., et al. 2018. Synthesis of Green Silica from Agricultural Waste by Sol-Gel Method. *Mater Today Proc.* **5(1)**:21861-21865.
- Thakur, A. and Kumar, A. 2021. Sustainable Inhibitors for Corrosion Mitigation in Aggressive Corrosive Media: A Comprehensive Study. *J. Bio-Tribo-Corrosion* **7(1)**:67-68.
- Umoren, S.A., Eduok, U.M., Solomon, M.M., et al. 2016. Corrosion Inhibition by Leaves and Stem Extracts of *Sida Acuta* for Mild Steel in 1M H<sub>2</sub>SO<sub>4</sub> Solution Investigated by Chemical and Spectroscopic Techniques. *Arabian Journal of Chemistry* **9(1)**:209-224.
- Uwaezuoke, N. 2022. Polymeric Nanoparticles in Drilling Fluid Technology. In *Drilling Engineering and Technology-Recent Advances, New Perspectives and Applications*, ed. M. Zoveidavianpoo, Chap. 1, 1-15. London: IntechOpen.
- Uwaezuoke, N., Okoro, V., Igwilo, K.C., et al. 2022. Characterization of Amuda-Isuochi Nigerian Clay Deposit for Potential Industrial Applications. *International Journal of Engineering Research in Africa* **62(1)**:1-18.

**Nnaemeka Uwaezuoke** is a Senior Lecturer at the Department of Petroleum Engineering, Federal University of Technology Owerri with Research Interest in drilling and well engineering. Uwaezuoke holds a Bachelor's degree in Petroleum Engineering from Federal University of Technology Owerri; Master's degree in Petroleum

Engineering from University of Stavanger, Norway; and a PhD degree in Petroleum Engineering from Federal University of Technology Owerri, Nigeria.

**Okon Emmanuel Onya** is a Graduate of Petroleum Engineering from the Department of Petroleum Engineering, Federal University of Technology Owerri, Nigeria, with research interest in drilling engineering and corrosion control.

**Nnaji Okechukwu Christopher** is a Graduate of Petroleum Engineering from the Department of Petroleum Engineering, Federal University of Technology Owerri with research interest in reservoir engineering and corrosion control.

**Chukwuebuka Francis Dike** is a Research Technologist at the Department of Petroleum Engineering, Federal University of Technology Owerri with research interest in drilling fluids, enhanced oil recovery, reservoir engineering and flow assurance. Dike holds a Bachelor's degree and Master's degree in Petroleum Engineering.

**Ibuchukwu Stanley Onwukwe** is a Professor at the Department of Petroleum Engineering, Federal University of Technology Owerri with research interest in reservoir engineering, enhanced oil recovery, natural gas engineering, petroleum production and petroleum economics. Onwukwe holds a Bachelor's, Master's and a PhD degree in Petroleum Engineering from Federal University of Technology Owerri, Nigeria.